Transmission of light through periodic arrays of sub-wavelength slits in metallic hosts

Y. Xie, A. R. Zakharian, J. V. Moloney, and M. Mansuripur

College of Optical Sciences, The University of Arizona, Tucson, Arizona 85721
xie@email.arizona.edu

Abstract: Using Bloch modes to study the extraordinary transmission of light through a periodic array of slits in a metallic host, we discuss the differing roles of surface plasmon polaritons and Wood's anomalies in the observed behavior of such structures. Under certain circumstances, the first few excited modes appear to play a decisive role in determining the transmission efficiency of the array. Surface plasmon excitations tend to reduce the transmissivity of a semi-infinitely thick slit array, yet, paradoxically, the same reduction can account for enhanced transmission in an array of finite thickness τ, provided that τ is tuned to a Fabry-Perot-like resonance between the entrance and exit facets of the slit array. At the Wood anomaly, power redistribution produces sharp peaks in the diffraction efficiencies of various reflected and transmitted orders of the semi-infinite structure. With skew incidence, the degenerate states split, resulting in two peaks and two valleys, as observed by Wood in his 1902 experiments.

©2006 Optical Society of America

OCIS codes: (050.1220) Apertures; (050.1960) Diffraction theory; (240.6680) Surface plasmons; (260.3910) Optics of metals; (310.2790) Guided waves.

References and links

1. T. W. Ebbesen, H. J. Lezec, H. F. Ghaemi, T. Thio, P. A. Wolff, "Extraordinary optical transmission through subwavelength hole arrays," Nature **39**, 667-669 (1998).
2. M. M. J. Treacy, "Dynamical diffraction explanation of the anomalous transmission of light through metallic gratings," Phys. Rev. B **66,** 195105-11 (2002).
3. H. J. Lezec and T. Thio, "Diffracted evanescent wave model for enhanced and suppressed optical transmission through subwavelength hole arrays," Opt. Express **12**, 3629-3651 (2004).
4. G. Gay, O. Alloschery, B. Viaris de Lesegno, C. O'Dwyer, J. Weiner, H. J. Lezec, "The optical response of nanostructured surfaces and the composite diffracted evanescent wave model," Nature Phys. **264**, 262 – 67 (2006).
5. S. H. Chang, S. Gray, and G. Schatz, "Surface plasmon generation and light transmission by isolated nanoholes and arrays of nanoholes in thin metal films," Opt. Express **13**, 3150-3165 (2005).
6. C. Genet, M. P. van Exter, and J. P. Woerdman, "Fano-type interpretation of red shifts and red tails in hole array transmission spectra," Opt. Communications **225**, 331 (2003).
7. Q. Cao and Ph. Lalanne, "Negative role of surface plasmons in the transmission of metallic gratings with very narrow slits," Phys. Rev. Lett. **88**, 057403(4) (2002).
8. Y. Xie, A. R. Zakharian, J. V. Moloney, and M. Mansuripur, "Transmission of light through a periodic array of slits in a thick metallic film," Opt. Express **13**, 4485 (2005)
9. J. A. Porto, F. J. García-Vidal, J. B. Pendry, "Transmission resonance on metallic gratings with very narrow slits," Phys. Rev. Lett. **83**, 02845(4) (1999).
10. J. Bravo-Abad, L. Martín-Moreno, F. J. García-Vidal, "Transmission properties of a single metallic slit: from the subwavelength regime to the geometrical-optics limit," Phys. Rev. E **69**, 26601(6) (2004).
11. Y. Xie, A.R. Zakharian, J. V. Moloney, M. Mansuripur, "Transmission of light through slit apertures in metallic films," Opt. Express **12**, 6106 (2004).
12. R. W. Wood, "On a remarkable case of uneven distribution of light in a diffraction grating spectrum," Proc. Phys. Soc. London **18**, 269-275 (1902).
13. R. W. Wood, "Anomalous diffraction gratings," Phys. Rev. **48**, 928-937 (1935).
14. H. Raether, Surface Plasmons on smooth and rough surfaces and on gratings, (Springer-Verlag, Berlin, 1986).
15. Ph. Lalanne, C. Sauvan, J. P. Hugonin, J. C. Rodier, and P. Chavel, "Perturbative approach for surface plasmon effects on flat interfaces periodically corrugated by subwavelength apertures," Phys. Rev. B **68**, 125404 (2003).
16. Ph. Lalanne, J. P. Hugonin, and J. C. Rodier, "Theory of Surface Plasmon Generation at Nanoslit Apertures," Phys. Rev. Lett. **95**, 263902 (2005).

#69390 - $15.00 USD Received 27 March 2006; revised 22 June 2006; accepted 22 June 2006
(C) 2006 OSA

17. M. G. Moharam, E. B. Grann, D. A. Pommet, and T. K. Gaylord, "Formulation for stable and efficient implementation of the rigorous coupled-wave analysis of binary gratings," J. Opt. Soc. Am. A **12**, 1068-76 (1995).
18. Ph. Lalanne and G. M. Morris, "Highly improved convergence of the coupled-wave method for TM polarization," J. Opt. Soc. Am. A **13**, 779-84 (1996).
19. J. D. Jackson, *Classical Electrodynamics*, Chapter 8, 3rd edition, Wiley, New York, 1999.
20. A. W. Snyder and J. D. Love, *Optical Waveguide Theory*, Chapman and Hall, London, 1983.
21. R. N. Bracewell, *The Fourier Transform and its Applications*, McGraw-Hill, New York, 1978.
22. Lord Rayleigh, "On the dynamic theory of gratings", Proc. R. Soc. A **79**, 399-416 (1907).
23. E. Noponen, "Electromagnetic Theory of Diffractive Optics," dissertation, Dept. of Technical Physics, Helsinki University of Technology, Finland (1994).
24. P. Edward, *Handbook of optical constants of solids*, 1st edition, Academic press, 1997.

1. Introduction

The extraordinary transmission of electromagnetic waves through single apertures or periodic arrays of such apertures has been the subject of theoretical and experimental investigations for several years [1-11]. Such enhanced transmissions should pave the way for the design of nano-photonic devices with novel functionality and high efficiency. A consensus, however, has not yet emerged as to the underlying mechanism(s) of the observed phenomena.

Treacy summarized three physical models in his 2002 paper [2], and his simulations focused on the validity of these theories with regard to the transmission properties of metallic gratings. Lezec *et al*. [3, 4] proposed a simplified variant on Treacy's dynamic diffraction theory, and presented experimental data in support of the role played in enhanced transmission by interference with evanescent modes on the surface. Chang *et al*. [5] presented a numerical study of subwavelength apertures in gold films, showing remarkable agreement with a model that exploits similarities with Fano resonances of atomic systems [6]. For the role of surface plasmon polaritons (SPP) in the transmission process, Cao and Lalanne [7] followed a strict definition and, using a rigorous coupled-wave analysis (RCWA), concluded that SPP plays a negative role in the transmission enhancement. In [8] we agreed with Cao and Lalanne, having investigated this problem with finite-difference-time-domain (FDTD) simulations. On the other hand, Porto *et al*. [9], arguing from their transfer-matrix-based calculations, believe that SPP excitation should help the transmission. For a single sub-wavelength slit aperture [10, 11], transmission of the TM mode turns out to be so high that SPP excitation alone may not suffice to explain the results. These contradictions in belief and discrepancies in analysis highlight the need for a satisfactory explanation of SPP-related phenomena. It is the intent of the present paper to address the aforementioned problem and, hopefully, to shed some light on the roots of the controversy.

The reason that Treacy [2] did not discuss the role of SPP in his paper might be that the concept has been used vaguely (though extensively) in discussing the interaction between light and metallic structures. In fact, a majority of the studies in this area do not even mention, let alone clarify, the connections among surface plasmons, the Wood anomalies [12, 13], and the high transmission efficiencies of slit arrays. In our view, a working model that does not address these phenomena collectively and coherently, cannot hope to clarify the prevailing discrepancies. We adopt Raether's definition of the SPP [14] throughout this paper. Accordingly, SPP is a localized electromagnetic wave at a dielectric-metal interface, formed by a single evanescent plane-wave on the dielectric side of the interface, and a single inhomogeneous plane-wave on the metal side. The continuity of the tangential *E*- and *H*-fields uniquely specifies the common (tangential) component of the *k*-vector for these two beams as $k_{spp} = k_o\sqrt{\varepsilon_m\varepsilon_d/(\varepsilon_m + \varepsilon_d)}$, where $k_o = 2\pi/\lambda_o$ is the propagation constant in vacuum, and ε_m and ε_d are the (relative) permittivities of the metal and the dielectric, respectively. (The surface plasmon resonance at $\omega_{sp} = \omega_P/\sqrt{2}$ must be distinguished from the SPP, which appears at frequencies below ω_{sp}. While the resonant SP, a collective oscillation of all surface electrons,

#69390 - $15.00 USD Received 27 March 2006; revised 22 June 2006; accepted 22 June 2006
(C) 2006 OSA

has a group velocity of zero, the SPP is a localized excitation that propagates with a finite group velocity as a guided surface mode.)

When a periodic array of slits (either empty or filled with a dielectric) is introduced in a semi-infinite metallic host, under certain circumstances, the electromagnetic waves excited at the entrance facet will have the SPP character. These waves, however, are not directly responsible for the electromagnetic transmission through the slits; there are other, so-called guided, modes that are also excited at the entrance facet, and these carry some of the incident energy into the depths of the slits. (In a metallic host, when the slit-width happens to be less than one half of one wavelength, there exists only one guided mode with TM polarization, and none with TE polarization.) The interplay between evanescent modes (including SPP), which remain confined to the entrance facet of the slit array, and guided mode(s), which propagate into the slits, determines the transmission efficiency of the array. (We use the term "guided mode" to refer exclusively to the electromagnetic mode that propagates within the slit and not, as done by some other authors, to mean the SPP.) Our calculations confirm that the excitation of SPP results in a substantial reduction of the transmission efficiency in semi-infinitely thick arrays of slits, whereas high transmissivities are generally associated with the onset of Wood's anomalies. Moreover, it will be shown that Wood's anomalies are not the exclusive domain of high transmission efficiencies.

In Section 2 we construct the Bloch modes of a slit array in order to study the transmission and diffraction efficiencies of the structure. A reason for using Bloch *modes* (instead of Bloch *waves*) is that, inside the periodic structure, such modes exist and propagate independently of all the other modes. In a semi-infinite slit array located in the half-space $z > 0$ and illuminated by a plane-wave arriving from the free space region $z < 0$, the strength of the various excited modes can be determined by matching the boundary conditions at the entrance facet of the slit array, namely, in the xy-plane located at $z = 0$. This is done in Section 3, where we minimize (simultaneously) the difference between the tangential E-fields, as well as that between the tangential H-fields, across the interface. The (complex) amplitudes of all the excited modes are thus determined and, with enough modes included in the calculation, the boundary conditions at $z = 0$ are satisfied.

When transmission through the slits is computed as a function of the period p of the array (all other parameters being kept constant), the excitation of SPP and the occurrence of Wood's anomaly will be seen to be vastly different phenomena insofar as the number and strength of excited Bloch modes are concerned. In Section 4, we analyze the modal content of reflected and transmitted beams, identify dominant modes, and explain their roles in enhancing or weakening the transmission under conditions that either favor the excitation of SPP or usher in the Wood anomalies. Section 5 provides a brief analysis of the SPP and Wood anomalies at oblique incidence. Final remarks and conclusions appear in Section 6.

2. Bloch modes of a periodic array of slits in a semi-infinite metallic host

Figure 1 shows a periodic array of slits in a metallic host occupying the half-space $z > 0$. The array is illuminated by a plane-wave from the free-space region above the surface, which surface is the xy-plane at $z = 0$. The host material is silver, the slits are empty (i.e., vacuum or air-filled), the incident wavelength is λ_o, the array periodicity along the y-axis is p, and the slit-width is w. We shall consider only the case of incident plane-waves whose propagation vector $\boldsymbol{k}$ lies in the yz-plane; these will be assumed to be linearly polarized within the plane of incidence; in other words, the incident plane-waves are transverse-magnetic (TM) or p-polarized. Although, for the most part, this paper will be concerned with a normally incident plane-wave polarized along the y-axis, (E_y, H_x), generalizing the method of analysis to oblique incidence is fairly straightforward; some numerical results pertaining to the case of oblique incidence are presented in Section 5.

Bloch modes exist within the periodic structure, in the region where $z > 0$, while ordinary homogeneous (i.e., propagating) and inhomogeneous (i.e., evanescent) plane-waves reside in the free-space region above the slit array, where $z < 0$. Our construction of the Bloch modes of the slit-array ensures that Maxwell's equations hold both within the slits and in the metallic

#69390 - $15.00 USD Received 27 March 2006; revised 22 June 2006; accepted 22 June 2006
(C) 2006 OSA

host, with boundary conditions satisfied on the slits' vertical walls. Matching the boundary conditions at the top surface, $z = 0$, leads to a determination of the (complex) amplitudes of the various excited modes that reside above and below the interface.

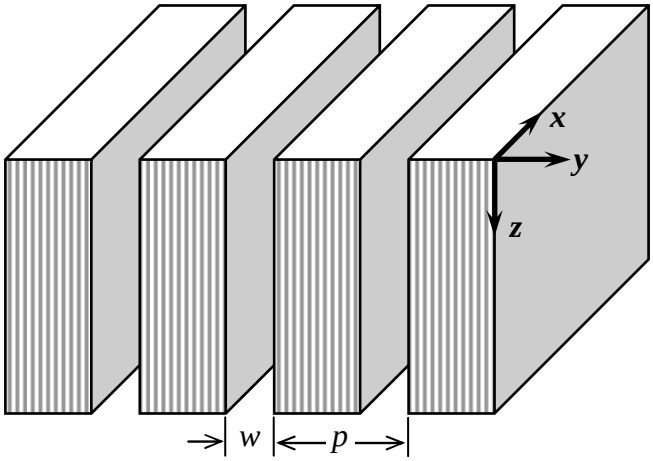

Fig. 1. A plane-wave illuminates, from the top, a semi-infinite array of slits in a metallic host (silver). The plane of incidence is yz, the vacuum wavelength of the incident beam is $\lambda_o = 1.0\mu m$, and the permittivity of silver at this frequency is $\varepsilon_m = -48.8 + i2.99$. The slit width is fixed at $w = 0.1\mu m$, but the array periodicity p is an adjustable parameter of our calculations ($0.4\mu m < p < 3.2\mu m$). Only TM modes (H_x, E_y, E_z) are considered.

Lalanne *et al*. [15, 16] have used a similar approach for metallic and dielectric gratings with only a few modes considered. We will extend their technique to slit arrays in a host medium of complex permittivity ε_m, and will include as many Bloch modes as needed to achieve convergence. In this section, we express the *E*- and *H*-fields inside the slits and within the metallic host as superpositions of inhomogeneous plane-waves, and solve the transcendental equation that results from the continuity of H_x and E_z on the slit walls. At normal incidence, the equations are somewhat simplified due to symmetry.

2.1 Transcendental equation for Bloch modes of the slit array

The natural modes within the free-space region $z < 0$ above the slit array are propagating as well as evanescent plane-waves (i.e., Rayleigh expansion, similar to RCWA method [17, 18]). To obtain the modes inside the periodic structure, one must solve Maxwell's equations for a slab waveguide with periodic boundary conditions. These solutions may be decoupled into TE (E_x, H_y, H_z) and TM (H_x, E_y, E_z) modes. The sole concern of the present paper is TM modes, as TE modes do not propagate through slits narrower than a half-wavelength. We express the *E*- and *H*-fields inside the slits – which are either empty or filled with a transparent material of dielectric constant ε_s – and also the fields in the metallic regions between adjacent slits as superpositions of two (generally inhomogeneous) plane-waves bouncing back and forth between the vertical walls. The *H*-field transmitted below the surface at $z = 0$ is thus written

$$H_{xT}^n(y,z) = \begin{cases} \exp(ik_0\sigma_z^n z)\{h_{1s}^n \exp[ik_0\sigma_{ys}^n(y+w/2)] + h_{2s}^n \exp[-ik_0\sigma_{ys}^n(y-w/2)]\}, & -\dfrac{w}{2} < y < \dfrac{w}{2} \\ \exp(ik_0\sigma_z^n z)\{h_{1m}^n \exp[ik_0\sigma_{ym}^n(y-w/2+p)] + h_{2m}^n \exp[-ik_0\sigma_{ym}^n(y+w/2)]\}, & \dfrac{w}{2} - p \le y \le -\dfrac{w}{2} \end{cases} \quad (1)$$

Here n is the mode index (1, 2, 3, …), $k_o = 2\pi/\lambda_o$ is the vacuum wave-number, σ_z^n is the n^{th} mode's propagation constant along the z-axis, the subscript s denotes the slit region, and the subscript m denotes the metallic host medium (i.e., cladding for the slit waveguides). Inside the slits $(\sigma_{ys}^n)^2 + (\sigma_z^n)^2 = \varepsilon_s$, where ε_s is the relative permittivity of the filling material, while

#69390 - $15.00 USD Received 27 March 2006; revised 22 June 2006; accepted 22 June 2006
(C) 2006 OSA

in the metal $(\sigma_{ym}{}^{n})^2 + (\sigma_z{}^{n})^2 = \varepsilon_m$, where ε_m is the relative permittivity of the host material. The horizontal component E_y and the vertical component E_z of the E-field are proportional to the partial derivatives of H_x with respect to z and y, respectively:

$$E_{yT}^n = \begin{cases} -\dfrac{1}{i\omega\varepsilon_s\varepsilon_0}\dfrac{\partial H_{xT}^n(y,z)}{\partial z}, & -\dfrac{w}{2} < y < \dfrac{w}{2} \\ -\dfrac{1}{i\omega\varepsilon_m\varepsilon_0}\dfrac{\partial H_{xT}^n(y,z)}{\partial z}, & \dfrac{w}{2} - p \le y \le -\dfrac{w}{2} \end{cases} \tag{2.a}$$

$$E_{zT}^n = \begin{cases} \dfrac{1}{i\omega\varepsilon_s\varepsilon_0}\dfrac{\partial H_{xT}^n(y,z)}{\partial y}, & -\dfrac{w}{2} < y < \dfrac{w}{2} \\ \dfrac{1}{i\omega\varepsilon_m\varepsilon_0}\dfrac{\partial H_{xT}^n(y,z)}{\partial y}, & \dfrac{w}{2} - p \le y \le -\dfrac{w}{2} \end{cases} \tag{2.b}$$

ε_o is the vacuum permittivity, and $\omega = 2\pi c/\lambda_o$ is the angular frequency of the incident beam. Defining $\Lambda = \exp(\mathrm{i}\, k_o p \sin\theta)$, where θ is the incident plane-wave's angle of incidence, the Bloch condition requires that

$$\begin{cases} H_{xT}^n(y+p,z) = \Lambda H_{xT}^n(y,z) \\ E_{zT}^n(y+p,z) = \Lambda E_{zT}^n(y,z) \end{cases} \tag{3}$$

Matching the tangential E- and H-fields at the vertical walls of the slits yields:

$$\begin{cases} H_{xT}^n|_{y=-w/2+} = H_{xT}^n|_{y=-w/2-} \\ E_{zT}^n|_{y=-w/2+} = E_{zT}^n|_{y=-w/2-} \\ H_{xT}^n|_{y=w/2-} = \Lambda H_{xT}^n|_{y=(w/2-p)+} \\ E_{zT}^n|_{y=w/2-} = \Lambda E_{zT}^n|_{y=(w/2-p)+} \end{cases} \tag{4}$$

These boundary conditions, when written out in matrix form, yield a 4×4 matrix equation for the H-field amplitudes (h_{1s}, h_{2s}, h_{1m}, h_{2m}) of the n^{th} mode, namely,

$$\begin{pmatrix} 1 & a & -b & -1 \\ \sigma_{ys}/\varepsilon_s & -a\sigma_{ys}/\varepsilon_s & -b\sigma_{ym}/\varepsilon_m & \sigma_{ym}/\varepsilon_m \\ a & 1 & -\Lambda & -b\Lambda \\ a\sigma_{ys}/\varepsilon_s & -\sigma_{ys}/\varepsilon_s & -\Lambda\sigma_{ym}/\varepsilon_m & b\Lambda\sigma_{ym}/\varepsilon_m \end{pmatrix} \begin{pmatrix} h_{1s} \\ h_{2s} \\ h_{1m} \\ h_{2m} \end{pmatrix} = 0 \tag{5}$$

In Eq. (5), $a = \exp(\mathrm{i}\, k_o \sigma_{ys} w)$ and $b = \exp[\mathrm{i}\, k_o \sigma_{ym} (p - w)]$. Existence of a non-trivial solution for (h_{1s}, h_{2s}, h_{1m}, h_{2m}) requires that the determinant of the coefficient matrix be zero. For each mode, therefore, the propagation constant $\sigma_z{}^{n}$ must satisfy the characteristic equation:

$$(a^2-1)(b^2-1)(\varepsilon_m^2\sigma_{ys}^2 + \varepsilon_s^2\sigma_{ym}^2) + 2\varepsilon_s\varepsilon_m\left[(a^2+1)(b^2+1) - 2ab(\Lambda + \Lambda^{-1})\right]\sigma_{ys}\sigma_{ym} = 0 \tag{6}$$

At normal incidence, $\Lambda = 1$ and the equations are simplified by virtue of symmetry. For even modes, $h_{1s} = h_{2s}$ and $h_{1m} = h_{2m}$, and the characteristic equation simplifies as follows:

$$\frac{\varepsilon_m\sigma_{ys}}{\varepsilon_s\sigma_{ym}} = \frac{(a+1)(1-b)}{(a-1)(1+b)} \tag{7}$$

#69390 - $15.00 USD Received 27 March 2006; revised 22 June 2006; accepted 22 June 2006
(C) 2006 OSA

2.2 Bloch mode profiles

The transcendental Eq. (6), or its simplified version at normal incidence, Eq. (7), can be solved by a brute force search of the complex plane for viable solutions for σ_z. We enumerate the solutions in such a way that lower-order modes will lose less power as they propagate along the *z*-axis; that is, σ_z will be ordered in accordance with the strength of its imaginary part. If the solutions include guided modes, these will constitute the least lossy modes of all.

For the first mode of a slit-array having $p = 0.9\mu m$, $w = 0.1\mu m$ at $\lambda_o = 1.0\mu m$ (normal incidence), we find $\sigma_z^{\,1} = 1.21 + 0.0066i$ (the only guided mode in this system); the small imaginary part ensures that, if the mode is successfully launched at the entrance facet, it will be detectable after traveling several tens of wavelengths (λ_o) along the *z*-axis. For this system, Fig. 2(a) shows the locations of σ_z for modes 2 through 30 in the complex plane; the corresponding plots for σ_{ys} and σ_{ym} are shown in Figs. 2(b, c); the arrows identify the direction of increasing mode number, from 2 to 30.

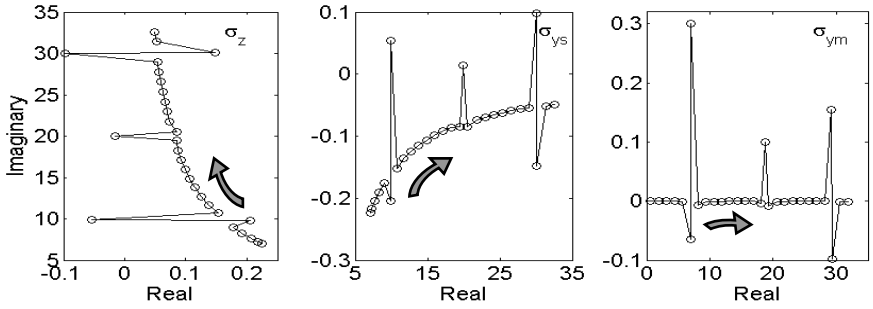

Fig. 2. Locations of σ_z, σ_{ys} and σ_{ym} in the complex-plane for mode-numbers 2 through 30, corresponding to a slit array having $p = 0.9\mu m$, $w = 0.1\mu m$ at $\lambda_o = 1.0\mu m$, normal incidence. The arrows point in the direction of increasing mode-number, from 2 to 30. The first mode, which is the only guided mode in this system, is off the scale and, therefore, not shown ($\sigma_z^{\,1} = 1.21 + 0.0066i$, $\sigma_{ys}^{\,1} = -0.012 + 0.68i$, $\sigma_{ym}^{\,1} = 0.21 + 7.1i$). The few abnormalities (i.e., departures from a smooth path) occur at regular intervals, with their $Imag[\sigma_z]$ separated by $\sim\lambda_o/w$. Abnormal modes are produced by lateral Fabry-Perot-like resonances within the slits.

Once σ_z is determined, the mode profiles $H_x(y, z)$, $E_y(y, z)$, $E_z(y, z)$ are readily calculated. Figure 3 shows profiles $|H_x(y, z = 0^+)|$ and $|E_y(y, z = 0^+)|$ of the first 10 Bloch modes for the $p = 0.9\mu m$, $w = 0.1\mu m$ slit array under normally-incident plane-wave ($\lambda_o = 1.0\mu m$). Each mode, of course, will decay exponentially along the propagation direction *z* in accordance with the factor $\exp(ik_o\sigma_z^{\,n} z)$. Similar profiles can be computed for other sets of parameter values.

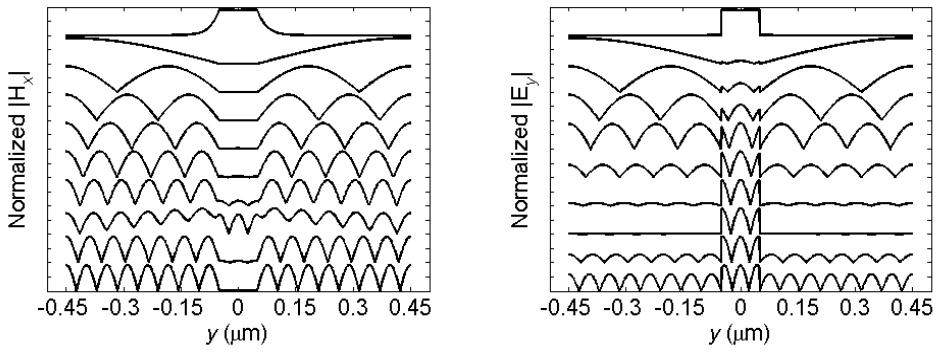

Fig. 3. The first ten modes of a slit array in a semi-infinite silver host ($p = 0.9\mu m$, $w = 0.1\mu m$, $\lambda_o = 1.0\mu m$, normal incidence). The magnitude of H_x is shown on the left, that of E_y on the right. The first mode (shown at the top) is the guided mode through the empty slits ($\varepsilon_s = 1.0$); all the other modes are highly damped along the *z*-axis. The mode profiles are similar to those computed by Treacy based on the RCWA method [2].

#69390 - $15.00 USD Received 27 March 2006; revised 22 June 2006; accepted 22 June 2006
(C) 2006 OSA

The $(n+1)^{st}$ mode typically has one more wiggle than the n^{th} mode in the metal on either side of the slit. Inside the slit, however, an additional wiggle appears only once every several modes. With an increasing period p, determination of the modes becomes more difficult as more roots σ_z of the transcendental Eq. (6) become available per unit area of the complex plane. When $w < \lambda_o/2$, the first mode can propagate deep into the slits, while all other modes exhibit large absorption along z. The mode amplitudes thus drop rapidly after propagating even a short distance; for higher-order modes this distance is much smaller than the skin-depth of the metallic host. The modes typically extend along y in the host material with fairly small attenuation, as can be inferred from the complex-plane distribution of σ_{ym} depicted in Fig. 2(c). These modes build up the charges and currents on the top surface of the metal, and contribute to the accumulated charges at the corners of the slits.

2.3 Orthogonality of Bloch modes

The mode profiles in the free-space region above the slit-array are simple sinusoids; as such, it can be shown that these modes are pairwise orthogonal [19]. In contrast, the modes below the surface, residing partly in the metal and partly in the free-space region of the slit, are *not* mutually orthogonal [20]. This can be seen in Fig. 4, which shows the magnitudes of the inner products of the first 60 modes for both H_x and E_y fields. (Inner products are defined as $\int H_x^n(y, 0)H_x^{m*}(y, 0)\,dy$ and $\int E_y^n(y, 0)E_y^{m*}(y, 0)\,dy$, with individual modes doubly normalized, i.e., $\int |H_x^n(y, 0)|^2\,dy = 1$ and $\int |E_y^n(y, 0)|^2\,dy = 1$.) Lack of orthogonality is particularly striking in the case of E_y profiles, where nearby modes exhibit a substantial degree of overlap. The apparent regularity of the inner products might signify a deep connection with the abnormal roots depicted in Fig. 2, although their relationship is not understood at present.

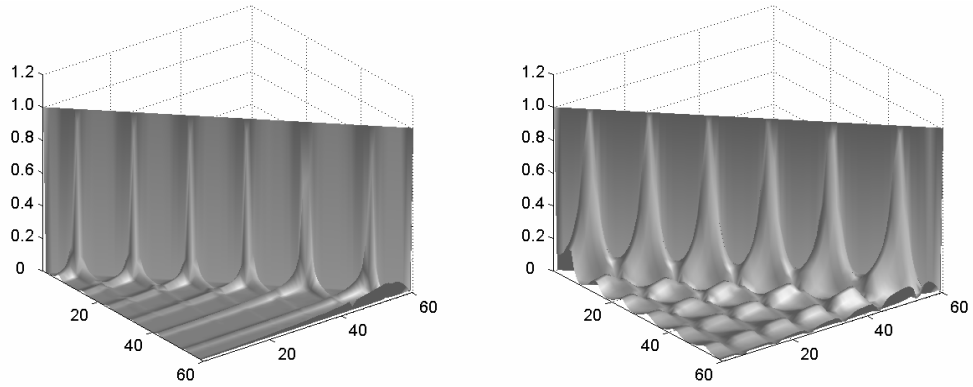

Fig. 4. Inner products of the first 60 modes for H_x (left) and E_y (right). While the H_x-fields of these modes are nearly pairwise orthogonal, the E_y-fields have substantial overlap with their neighboring modes. Each mode is doubly normalized, i.e., $\int |H_x^n(y, 0)|^2\,dy = \int |E_y^n(y, 0)|^2\,dy = 1$.

3. Excitation of Bloch modes by an incident plane wave

To calculate the coupling coefficients, one needs the modes of the free-space region above the slit array, which are then used in a Rayleigh expansion of the electromagnetic field in the region $z < 0$. These include both homogeneous and inhomogeneous plane-waves, which are expressed by the general form:

$$H_{xR}^n(y, z) = \exp\left[ik_0\left(\sigma_z'^n z + \sigma_y'^n y\right)\right] \tag{8}$$

In the above equation, n is the mode number $(0, \pm1, \pm2, \pm3, \ldots)$, $\sigma'_y{}^n = \sin(\theta) + n\lambda_o/p$, and $(\sigma'_y{}^n)^2 + (\sigma'_z{}^n)^2 = 1$. (The primes distinguish σ_y, σ_z from similar symbols used for the slit array in Section 2.) The E-field can be obtained in the same way as before, from Eq. (2). At normal incidence, where $\theta = 0°$, symmetry allows only even modes, namely,

#69390 - $15.00 USD Received 27 March 2006; revised 22 June 2006; accepted 22 June 2006
(C) 2006 OSA

$$H_{xR}^{n}(y,z)=\exp\left[ik_0\left(\sigma_z'^{n}z+\sigma_y'^{n}y\right)\right]+\exp\left[ik_0\left(\sigma_z'^{n}z-\sigma_y'^{n}y\right)\right] \tag{9}$$

To match the boundary conditions at $z = 0$, H_x and E_y in the free-space region $z < 0$ – where the incident plane-wave (H_{xI}, E_{yI}, E_{zI}) must be added to the sum of homogeneous and evanescent reflected modes – are set equal to the corresponding fields resulting from a superposition of the excited Bloch modes in the $z > 0$ region of the slit array, that is,

$$\begin{aligned} H_{xI}+\sum_{n=1}^{N}C_R^nH_{xR}^n&=\sum_{n=1}^{N}C_T^nH_{xT}^n\\ E_{yI}+\sum_{n=1}^{N}C_R^nE_{yR}^n&=\sum_{n=1}^{N}C_T^nE_{yT}^n \end{aligned} \tag{10}$$

In Eq. (10), ${C_R}^n$ and ${C_T}^n$ are the (complex) coefficients of the n^{th} reflected and transmitted modes, respectively. Equation (10) may be further simplified by moving all the terms to the left-hand-side, that is,

$$\begin{aligned} H_{xI}-\sum_{n=1}^{2N}C_nH_x^n&=0\\ E_{yI}-\sum_{n=1}^{2N}C_nE_y^n&=0 \end{aligned} \tag{11}$$

Here $\{C_n\}=\{-{C_R}^n,{C_T}^n\}$, $H_x^n=\{{H_{xR}}^n,{H_{xT}}^n\}$, and $E_y^n=\{{E_{yR}}^n,{E_{yT}}^n\}$. The above equations must hold at all points of the [0, p] interval along the y–axis. The total number of modes, $2N$, included in these calculations is equally divided between reflected and transmitted modes.

3.1 The method of least squares

We use the "least squares" method of finding the modal coefficients $\{C_n\}$ by minimizing the integral of the squared modulus of the mismatch at the interface. The mismatch arises from the difference between the E_y-field profiles just above ($z = 0^-$) and just below ($z = 0^+$) the interface, as well as the difference between the H_x-field profiles in these two (adjacent) regions. We fix the number of modes in each region at some desired value N. (The mismatch should decline as more modes are incorporated.) The least-squares error may be written

$$Error=\int_{-p/2}^{p/2}\{Z_0^2\,|H_{xI}-\sum_{n=1}^{2N}C_nH_x^n|^2+|E_{yI}-\sum_{n=1}^{2N}C_nE_y^n|^2\}\mathrm{d}y \tag{12}$$

Here $C_n = C_n' + \mathrm{i}C_n''$ is the (initially unknown) coefficient of the n^{th} excited mode. Since in the MKSA system of units the E-field magnitude is generally greater than that of the H-field, we have used the weighting factor $Z_o = \sqrt{\mu_o/\varepsilon_o} \approx 377\ \Omega$ to balance the contributions of the two fields to the computed mismatch. For a total of $2N$ modes, there are $4N$ real-valued unknowns $\{C_n', C_n''\}$. Setting to zero the derivative of the *Error* function with respect to each unknown, namely, $\partial Error/\partial C_n' = 0$ and $\partial Error/\partial C_n'' = 0$, we find the following $2N$ equations for the $2N$ complex unknowns $\{C_n\}$:

$$\sum_{n=1}^{2N}C_n\int_{-p/2}^{p/2}\left(Z_0^2H_x^{j*}H_x^n+E_y^{j*}E_y^n\right)dy=\int_{-p/2}^{p/2}\left(Z_0^2H_x^{j*}H_{xI}+E_y^{j*}E_{yI}\right)dy \tag{13}$$

Here j, ranging from 1 to $2N$, is the index of the unknown coefficient, C_j, with respect to which the partial derivatives were evaluated. Equation (13), a set of $2N$ linear equations in $2N$ unknowns, may be written in matrix form, then solved by inverting the coefficients matrix.

The reflection and transmission coefficients for each mode, R_n and T_n, as well as the total reflected and transmitted optical power, R and T, may be computed using the corresponding component S_z of the Poynting vector $\boldsymbol{S}$ along the z-axis, that is,

#69390 - $15.00 USD Received 27 March 2006; revised 22 June 2006; accepted 22 June 2006
(C) 2006 OSA

$$R_n = \frac{\int_{-p/2}^{p/2} \mathrm{Re}\left[C_R^n E_{yR}^n \times (C_R^n H_{xR}^n)^* \right] dy}{\int_{-p/2}^{p/2} \mathrm{Re}\left(E_{yI} \times H_{xI}^{\ *} \right) dy} \tag{14.a}$$

$$T_n = \frac{\int_{-p/2}^{p/2} \mathrm{Re}\left[C_T^n E_{yT}^n \times (C_T^n H_{xT}^n)^* \right] dy}{\int_{-p/2}^{p/2} \mathrm{Re}\left(E_{yI} \times H_{xI}^{\ *} \right) dy} \tag{14.b}$$

$$T = \frac{\int_{-p/2}^{p/2} \mathrm{Re}\left[\sum_{n=1}^{N} C_T^n E_{yT}^n \times \sum_{n=1}^{N} (C_T^n H_{xT}^n)^* \right] dy}{\int_{-p/2}^{p/2} \mathrm{Re}\left(E_{yI} \times H_{xI}^{\ *} \right) dy} \tag{14.c}$$

In the free-space region above the interface, $R_n = 0$ for the evanescent modes, while, for propagating modes, R_n is the n^{th} order diffraction efficiency. Orthogonality of the modes in this region allows one to obtain the total reflectance R by summing the various R_n. In transmission, however, the various Bloch modes are not mutually orthogonal, and the total transmissivity must be computed directly by evaluating the z-component of the Poynting vector, as given by Eq. 14(c). While the transmitted guided mode loses its energy slowly to the vertical slit walls, the non-propagating modes of the slit array deposit their entire energy in a thin layer near the top surface of the metallic structure.

3.2. Convergence

For the previously studied slit array ($p = 0.9\mu m$, $w = 0.1\mu m$, $\lambda_o = 1.0\mu m$, normal incidence), Fig. 5 shows the E_y and H_x field profiles (on both sides of the $z = 0$ interface) with $N = 80$ modes included in the computation. The match is excellent, both in the slit region and over the metal surface. The difference between the incident power and the computed $R + T$ was found to be less than 0.3%. Although the high-frequency oscillations of E_y within the slit may, in part, be a manifestation of the Gibbs phenomenon [21], the sharp peaks at the slit edges are real and represent the significant accumulation of electrical charge on these sharp corners.

(**A note on the Gibbs phenomenon**: When a discontinuous function is reconstructed from its own Fourier transform, there occur oscillations on both sides of the discontinuity. Although these oscillations get compressed around the discontinuous point as more and more terms are included in the inverse Fourier series, the magnitude of the oscillations never reduces to zero, their peak remaining around 9% of the magnitude of the discontinuity.)

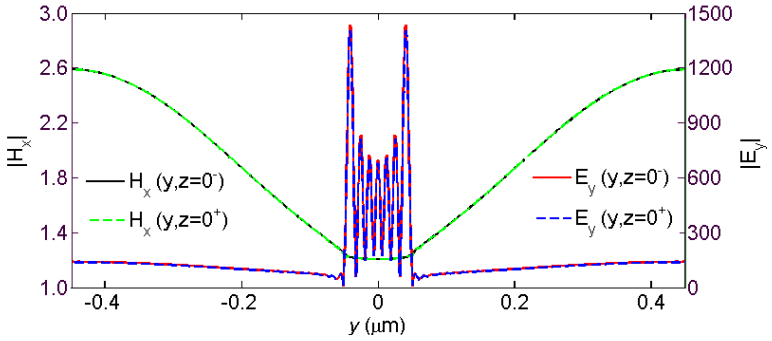

Fig. 5. Profiles of H_x and E_y across a full period of the slit array ($p = 0.9\mu m$, $w = 0.1\mu m$, $\lambda_o = 1.0\mu m$, normal incidence), with $N = 80$ modes used to reduce the mismatch at the interface. Excellent agreement is observed between the fields just above the surface (black for H_x , red for E_y) and those just beneath the surface (green for H_x , blue for E_y).

We also computed the various mode amplitudes $|C_n|$ as functions of N (the number of modes on each side of the $z = 0$ interface used to minimize the mismatch). Figure 6(a) shows the amplitude variations of the first five Bloch modes of the slit-array versus N, indicating that the mode coefficients stabilize after incorporating ~10−15 modes on each side of the

#69390 - $15.00 USD Received 27 March 2006; revised 22 June 2006; accepted 22 June 2006
(C) 2006 OSA

interface. Figure 6(b) shows the magnitudes of the first 25 Bloch modes of the slit-array when a total of $N = 80$ modes are used to match the boundary conditions. It is readily observed that the mode amplitudes are strong for the low-order modes (i.e., dominant modes), while higher-order modes are fairly weak. The solution converges rather slowly after the first few tens of modes, which is reminiscent of the RCWA behavior [17, 18].

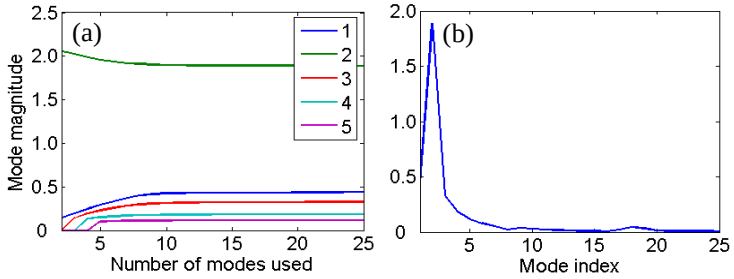

Fig. 6. (a) Magnitudes of the first five Bloch modes of the slit array ($C_T{}^1$,…, $C_T{}^5$) as functions of the total number of modes N used to minimize the mismatch between E_y and H_x across the $z = 0$ interface. (b) Magnitudes of the first 25 Bloch modes of the slit array, with $N = 80$ modes used to minimize the mismatch. ($p = 0.9\,\mu$m, $w = 0.1\,\mu$m, $\lambda_o = 1.0\,\mu$m, normal incidence.)

4. Transmittance of the slit array

Computed transmission efficiencies of a semi-infinite slit-arrays in silver having $w = 0.1\mu$m at $\lambda_o = 1.0\ \mu$m (normal incidence) versus the period p (ranging from 0.4μm to 3.2μm) are shown in Fig. 7. The blue curve represents the transmittance T_1 of the guided mode only, whereas the red curve corresponds to the total transmission efficiency T, which includes contributions by all the Bloch modes of the slit array. The non-guided modes of the array are, of course, absorbed within the first few nanometers upon entering the top facet of the metallic medium.

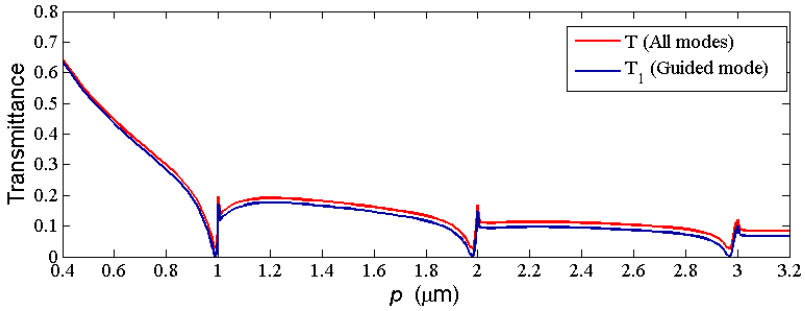

Fig. 7. Transmitted optical power (normalized by the incident power) versus the period p of a slit array in silver over the range $p = 0.4 – 3.2\ \mu$m ($w = 0.1\ \mu$m, $\lambda_o = 1.0\ \mu$m, normal incidence). The blue curve represents the transmissivity T_1 of the guided mode only (evaluated at $z = 0^+$), whereas the red curve shows the total transmissivity T when all modes up to and including $N = 80$ are considered. The difference between the two curves is the optical power absorbed near the entrance facet. Three sets of anomalies appear at and around $p = \lambda_o$, $2\lambda_o$, and $3\lambda_o$.

Starting at $p = 0.4\mu$m, both T and T_1 gradually decline to almost zero at $p = 0.99\mu$m, which is just below the Wood anomaly at $p = 1.0\mu$m. The transmission then climbs rapidly to a local maximum at $p = 1.0\mu$m, and falls immediately afterward. Subsequently, $T(p)$ and $T_1(p)$ repeat this behavior (decline followed by a sharp rise and a local peak) for $p = 1.0 – 2.0\mu$m and $p = 2.0 – 3.0\mu$m. The minima of T occur at those values of p that are generally associated with the excitation of SPP, i.e., when p becomes an integer-multiple of the SPP wavelength $\lambda_{spp} = \lambda_o\, Real\,[\sqrt{(1+\varepsilon_m)/\varepsilon_m}]$. In the present case, $\lambda_{spp} \approx 0.99\mu$m.

It must be mentioned that, within the numerical accuracy of our calculations, the guided mode's amplitude $C_T{}^1$ (hence the associated transmissivity T_1) is extremely small, although

#69390 - $15.00 USD Received 27 March 2006; revised 22 June 2006; accepted 22 June 2006
(C) 2006 OSA

not exactly zero, at $p = m\lambda_{spp}$ (m an integer). For m = 1, 2, 3, we examined the neighborhood of each such point carefully, and found that the minimum of T_1 in each case occurs at $p = m\lambda_{spp}$, with T_1 rising rapidly when the period p deviates, ever so slightly, from $m\lambda_{spp}$.

4.1. Modal analysis of the anomalies

To understand the nature of the anomalous behavior depicted in Fig. 7, we investigate the modal content of the reflected and transmitted beams at and around $p = \lambda_o$ and $p = 2\lambda_o$. For this discussion, the mode-numbering scheme is as follows: In transmission, modes 1 through 5 are the top five modes depicted in Fig. 3 (albeit for the relevant value of the period p); these are the five least lossy modes, starting with the guided mode as #1. In reflection, the first mode is the plane-wave directly reflected from the entrance facet of the slit array; this corresponds to the mode described by Eq. (8) with $n = 0$. The second mode is the sum of the two plane-waves in Eq. (8) having $n = \pm 1$; the left-right symmetry at normal incidence allows us to combine these two plane-waves into a single mode, as in Eq. (9). The third reflected mode is the sum of the two plane-waves having $n = \pm 2$, and so on.

Table I shows the magnitudes of the first few reflected and transmitted modes in the vicinity of $p = \lambda_o$. The case of $p = 0.8\mu m$ represents the normal behavior of the slit array, where a good mix of modes is excited on both sides of the interface. As p approaches $\lambda_{spp} = 0.99\mu m$, however, most of the modes diminish, leaving the normally reflected plane-wave (#1) plus a single evanescent mode (#2) in the region above the slit array, and essentially nothing but two non-propagating Bloch modes (#2 and #3) within the slit array. The single evanescent mode above the array (#2 in reflection) is, of course, characteristic of an excited SPP at a flat metal surface (with no slits), and the two Bloch modes of the slit array (transmitted modes #2 and #3) in combination resemble the requisite SPP excitation beneath a flat metal surface (again with no slits).

Table I. Magnitudes of the first five modes (both above and below the $z = 0$ interface) in the vicinity of $p = \lambda_o$, corresponding to the first anomaly depicted in Fig. 7 ($w = 0.1$ μm, $\lambda_o = 1.0$ μm, normal incidence).

p (μm)	***T***	***R***	**Transmitted mode magnitude**					**Reflected mode magnitude**				
			#1	#2	#3	#4	#5	#1	#2	#3	#4	#5
0.80	0.30	0.70	0.54	1.72	0.39	0.21	0.13	0.83	0.48	0.12	0.07	0.04
0.95	0.13	0.87	0.33	2.07	0.24	0.14	0.09	0.93	0.90	0.09	0.05	0.03
0.97	0.08	0.92	0.23	2.21	0.18	0.10	0.07	0.96	1.09	0.07	0.04	0.02
0.98	0.05	0.95	0.15	2.30	0.18	0.06	0.04	0.98	1.22	0.04	0.02	0.01
0.99	0.03	0.97	0.02	**2.39**	**0.27**	0.03	0.01	**0.99**	**1.39**	0.00	0.00	0.00
1.00	0.20	0.80	0.42	2.18	0.62	0.22	0.13	0.90	1.40	0.12	0.07	0.04
1.01	0.14	0.86	0.35	1.94	0.37	0.17	0.11	0.87	0.84	0.10	0.06	0.04
1.05	0.17	0.83	0.40	1.82	0.37	0.19	0.12	0.86	0.55	0.12	0.07	0.04

The top row in Fig. 8 shows plots of $|H_x(y, z = 0^+)|$ and $|E_y(y, z = 0^+)|$ over a full period at the $z = 0$ interface ($p = 0.99\mu m$). The green curve contains only the first 3 transmitted modes, while the blue curve is a superposition of all 80 modes. The net effect is that, at $p = 0.99\mu m$, the few excited modes of the structure conspire to "hide" the presence of the slits, making the slit array behave as if the slits did not exist. With the slits all but wiped out from the picture, the handful of excited modes (plus the incident beam, of course) manage to satisfy the boundary conditions at the $z = 0$ interface. The guided mode (#1 in transmission) is excited only weakly ($C_T^1 = 0.02$), and, with the exception of the residual absorption loss at the metal surface ($T \approx 3\%$), the incident beam is nearly fully reflected ($R \approx 97\%$).

#69390 - $15.00 USD Received 27 March 2006; revised 22 June 2006; accepted 22 June 2006
(C) 2006 OSA

The Wood anomaly was first observed by R. W. Wood in 1902 [12], and explained by Lord Rayleigh in his dynamic theory of diffraction published in 1907, where it was applied to a similar phenomenon in acoustics [22]. Subsequently, Wood investigated the phenomenon in more detail in 1935 [13]. Following Rayleigh, it is now generally accepted that the local peak in the diffraction efficiency at $p = \lambda_o$ is caused by a redistribution of energy due to the passing-off of the evanescent mode at grazing angle along the interface [23]. Table I shows that at $p = \lambda_o$ many modes are once again necessary to yield a good match at the $z = 0$ interface, and the graphs in the second row of Fig. 8 confirm the inadequacy of the first few modes to accomplish this task all by themselves. In going from $p = \lambda_{spp}$ to $p = \lambda_o$, the guided mode (#1 in transmission) suddenly rises to significance, the specularly reflected mode (#1 in reflection) weakens substantially, and the $\pm 1^{st}$ order diffracted beams (#2 in reflection), while remaining strong, switch from evanescence to propagating status. This upsets the balance of the *E*- and *H*-fields at the interface, thus requiring the excitation of many higher-order modes to restore the balance.

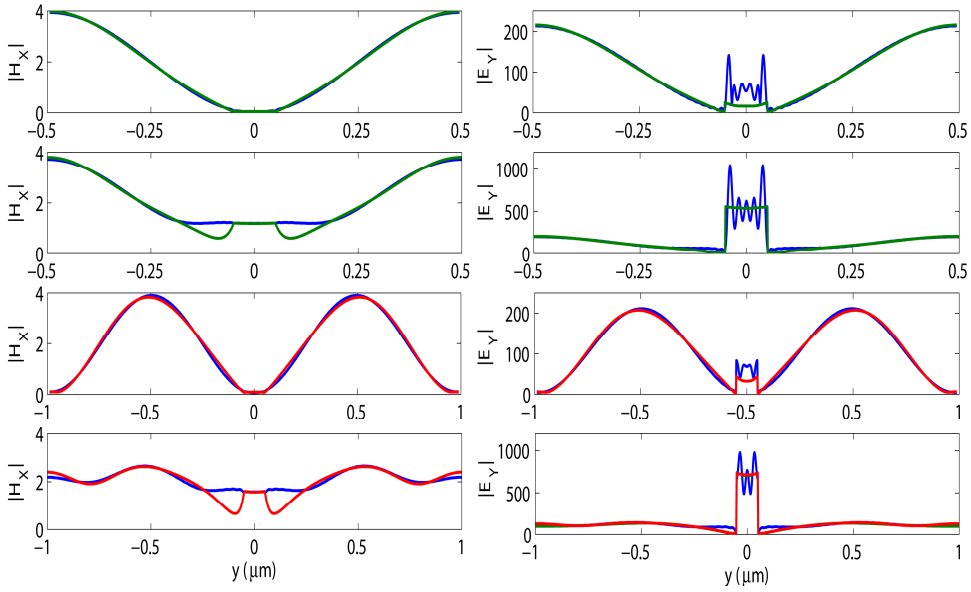

Fig. 8. Magnitudes of the tangential fields beneath the surface (H_x on the left, E_y on the right) across a full period p for four different slit arrays: from top to bottom, $p = \lambda_{spp}$, λ_o, $2\lambda_{spp}$, $2\lambda_o$; in all cases $w = 0.1$ μm, and $\lambda_o = 1.0$ μm at normal incidence. The mode amplitudes are computed using a total of $N = 80$ modes in each case. The depicted profiles show the superposition of all 80 modes (blue), as well as partial reconstructions containing only the first 3 modes (green), or the first 4 modes (red).

Table II shows the modal content of the reflected and transmitted beams in the vicinity of the anomaly at $p = 2\lambda_o$. In general, as in the case of $p < \lambda_{spp}$, many modes are needed to achieve a good match at the $z = 0$ interface. However, As p approaches $2\lambda_{spp} = 1.98$μm from below, the guided mode (#1 in transmission) is extinguished, the specularly reflected mode (#1 in reflection) gains prominence, the $\pm 1^{st}$ order diffracted beams (#2 in reflection) nearly vanish, and the evanescent mode with the resonant SPP frequency (#3 in reflection) rises high above all other evanescent modes in the free-space region $z < 0$. The first few Bloch modes of the slit array (#2, 3, 4 in transmission) are then needed to match the boundary conditions at the $z = 0$ interface, as can be readily observed in the $|H_x(y, z = 0^+)|$ and $|E_y(y, z = 0^+)|$ plots of Fig. 8, third row. Once again, as in the case of $p = \lambda_{spp}$, it is seen that at $p = 2\lambda_{spp}$ the SPP excitation (most readily recognized in the dominance of the reflected mode #3), masks the presence of the slits, thus preventing the excitation of the guided mode (#1 in transmission), and returning nearly all the incident optical power via specular reflection ($R \approx 97\%$).

#69390 - $15.00 USD Received 27 March 2006; revised 22 June 2006; accepted 22 June 2006
(C) 2006 OSA

Table II. Magnitudes of the first five modes (both above and below the $z = 0$ interface) in the vicinity of $p = 2\lambda_o$, corresponding to the second anomaly depicted in Fig. 7 ($w = 0.1$ μm, $\lambda_o = 1.0$ μm, normal incidence).

p (μm)	T	R	Transmitted mode magnitude					Reflected mode magnitude				
			#1	#2	#3	#4	#5	#1	#2	#3	#4	#5
1.80	0.14	0.86	0.35	1.74	0.70	0.23	0.17	0.92	0.15	0.37	0.10	0.06
1.95	0.06	0.94	0.21	1.80	1.12	0.18	0.09	0.96	0.09	0.88	0.07	0.04
1.97	0.04	0.96	0.10	1.83	1.34	0.29	0.06	0.98	0.04	1.17	0.04	0.02
1.98	0.03	0.97	0.02	**1.85**	**1.46**	**0.42**	0.08	**0.99**	0.01	**1.37**	0.01	0.00
1.99	0.06	0.94	0.19	1.84	1.45	0.59	0.17	0.97	0.07	1.46	0.06	0.04
2.00	0.17	0.83	0.39	1.74	0.83	0.61	0.25	0.90	0.15	0.93	0.14	0.08
2.01	0.11	0.89	0.31	1.75	0.75	0.38	0.18	0.92	0.12	0.60	0.11	0.06
2.02	0.11	0.89	0.31	1.75	0.72	0.34	0.17	0.92	0.12	0.51	0.11	0.06
2.05	0.11	0.89	0.31	1.75	0.68	0.31	0.17	0.92	0.12	0.39	0.11	0.07

As p increases beyond $2\lambda_{spp}$, the arrival of the second Wood anomaly at $p = 2\lambda_o = 2.0$μm once again wreaks havoc on the balance of the fields at the $z = 0$ boundary, throwing a large fraction of the incident optical power into the guided mode (#1 in transmission) and the $\pm 1^{st}$ order diffracted modes (#2 in reflection). The first few modes are no longer sufficient to satisfy the boundary conditions at the $z = 0$ interface, thus necessitating the excitation of higher order modes, as shown in Fig. 8, bottom row.

5. Oblique incidence

We investigate the behavior of a slit array ($p = 1.2$μm, $w = 0.1$μm) in a semi-infinite silver host in the wavelength range $\lambda_o = 0.4 - 0.7$μm at oblique incidence. Silver's permittivity in the considered range is interpolated linearly from known discrete values [24], and the incidence angles are fixed at $\theta = 0°$, 2°, and 4°. Computed plots of transmittance T, specular reflectance R_o, and the $\pm 1^{st}$ order reflected diffraction efficiencies $R_{\pm 1}$ are plotted versus λ_o in Fig. 9. A remarkable feature of these curves is that the transmittance T and the $\pm 1^{st}$ order diffraction efficiencies $R_{\pm 1}$ show very similar behavioral patterns. The anomalies are sharp and strong in the vicinity of $\lambda_o = p/2 = 0.6$μm, and less so around $\lambda_o = p/3 = 0.4$μm, indicating that a larger distance (in units of λ_o) between adjacent slits tends to reduce the effects of interference among the slits. We concentrate our attention where the anomalies are strong, i.e., at $\lambda_o \sim 0.6$μm.

For skew illumination, note that the maxima and minima of reflection and transmission are split into two sets, rather than simply shifting their positions relative to those corresponding to normal incidence. This is because the Bloch modes of the slit array have two sets of solutions, one with $|h_{1m}| > |h_{2m}|$, the other with $|h_{1m}| < |h_{2m}|$; see Eq. (1). Denoting the incidence wavelengths corresponding to the Wood and SPP anomalies by λ_{Wood} and λ_{spp}, their values may be calculated from:

$$\sin\theta + m\,(\lambda_{\text{Wood}}/p) = \pm 1 \tag{15}$$

$$\sin\theta + m\,(\lambda_{spp}/p) = \pm\, n_{spp}(\lambda) \tag{16}$$

With $m = \pm 2$ and $n_{spp} = Real[\sqrt{\varepsilon_d\,\varepsilon_m/(\varepsilon_d + \varepsilon_m)}] \approx 1.033$, we find in the case of $\theta = 2°$, $\lambda_{\text{Wood}} = 0.6 \pm 0.02$μm, $\lambda_{spp} = 0.62 \pm 0.02$μm, and in the case of $\theta = 4°$, $\lambda_{\text{Wood}} = 0.6 \pm 0.04$μm, $\lambda_{spp} = 0.62 \pm 0.04$μm, in agreement with the numerical computation results depicted in Fig. 9. We will present a more detailed discussion of oblique incidence in a forthcoming paper.

#69390 - $15.00 USD Received 27 March 2006; revised 22 June 2006; accepted 22 June 2006
(C) 2006 OSA

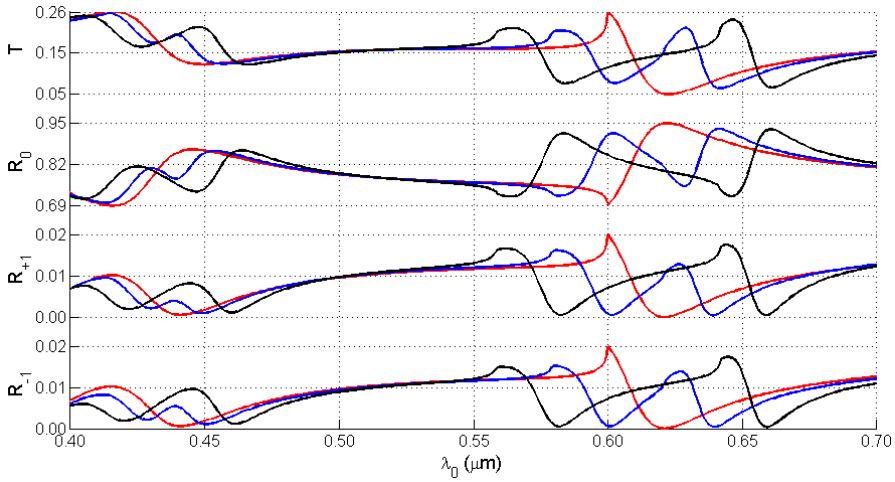

Fig. 9. Plots of total transmission efficiency T, as well as reflection efficiencies R_o, $R_{\pm 1}$ of the 0^{th} and $\pm 1^{st}$-order diffracted beams, as functions of the wavelength λ_o. The array periodicity and slit-width are fixed at p = 1.2μm, w = 0.1μm, respectively. The incidence angle is $\theta = 0°$ (red), $\theta = 2°$ (blue), and $\theta = 4°$ (black).

6. Concluding remarks

We have used the Bloch modes of a slit array in a semi-infinite metallic host to investigate the transmission anomalies of TM-polarized light through sub-wavelength slits in general, and the occurrence of high transmission under resonance conditions, in particular. We solved Maxwell's equations and calculated the reflection and transmission efficiencies for periodic arrays of slits illuminated with plane-waves at different angles of incidence. The set of anomalies (including the SPP resonance and the Wood anomaly) that shows up at normal incidence, splits into two sets at skew angles. The results indicate that, under most circumstances, there exists a fairly strong transmission through the slits, but the excitation of SPP at the entrance facet of the array results in a substantial reduction in transmission.

It must be noted, however, that the reduced transmissivity of semi-infinite slits under conditions that promote the excitation of SPP in no way contradicts the enhanced transmission of slit arrays in metallic films of finite thickness under the same conditions [7-11, 15]. In a film of finite thickness τ, an altogether different kind of resonance can take place in the cavity formed within the slit waveguide. The guided mode bounces back and forth between the entrance and exit facets of the slit (i.e., at the top and bottom facets of the metal film, separated by a distance τ), building strength in exactly the same way as the light trapped between the mirrors of a Fabry-Perot resonator gains strength by multiple reflections. The low transmissivity of the semi-infinite slit array (i.e., $\tau = \infty$) is, therefore, a necessary condition for the strong build-up of trapped light in a slit array of finite thickness. As the period p of a given array moves closer to λ_{spp}, the semi-infinite array becomes less transmissive, but, by the same token, the transmissivity of a finite thickness array (having the same values of p and w) can become extremely large if the Fabry-Perot resonance condition is satisfied, namely, $\phi_r + 2\pi\tau/\lambda = m\pi$, where ϕ_r is the phase acquired by the guided mode upon internal reflection from the top (or bottom) of the slit, λ is the guided mode's propagation wavelength, and m is an integer. This behavior, which has been extensively studied by Lalanne *et al*. [15, 16], was also observed in our previously reported numerical simulations [8].

Acknowledgments

We are grateful to John Weiner, Philippe Lalanne, Moysey Brio, Krishna Gundy and Hongbo Li for helpful discussions. This work has been supported by the AFOSR contracts F49620-03-1-0194, FA9550-04-1-0213, FA9550-04-1-0355 awarded by the Joint Technology Office.

#69390 - $15.00 USD Received 27 March 2006; revised 22 June 2006; accepted 22 June 2006
(C) 2006 OSA